Efficient CW Nd:YLF laser in-band Diode-pumped at 908 nm and its thermal lensing

By

Zohreh Sedaghati

A thesis submitted to the Faculty of Graduate Studies of

The University of Manitoba

In partial fulfillment of the requirements of the degree of

MASTER OF SCIENCE

Department of Electrical and Computer Engineering

University of Manitoba

Winnipeg

Abstract

Diode-pumped solid-state lasers are highly recommended for a variety of industrial and scientific applications as they can offer high efficiency and excellent beam quality. However, power scaling of these lasers is a challenging task. The main limitation in power scaling of famous neodymium doped lasers such as Nd:YVO_4 is the thermal lensing effect. Thermal lensing degrades the output beam quality and in extreme cases can result in crystal fracture. One potential solution to this problem is to reduce the induced heat load inside the gain media by decreasing the quantum defect. This was demonstrated successfully for the Nd:YVO_4 laser by pumping the laser at a long wavelength of 914 nm instead of the traditional pumping at 808 nm wavelength.

Among the Nd-doped crystals operating in the near infrared range, the crystal of yttrium lithium fluoride (Nd:YLF) is another interesting gain medium as it has the benefits of natural birefringence (can generate naturally polarized laser beam), negative *dn/dT* (reduces thermal effects) and long upper level lifetime (in favor of Q-switched operation).

In this work we used a long wavelength pumping approach and for the first time examined the performance of a continuous-wave Nd:YLF laser at 1047 nm under 908 nm diode pumping. This pumping wavelength reduced the quantum defect by 50% as compared to the conventional 808 nm pumping. The laser produced an output power of 850 mW at 1047 nm with excellent beam quality and 625 mW at 1053 nm. The slope efficiency was ~73.9% and 46% for 1047 and 1053 nm, respectively. Therefore, a considerable power scaling is possible for Nd:YLF crystals owing to the strongly reduced quantum defect and, hence, thermal lensing.

Acknowledgements

I would like to express my sincere gratitude to my advisor Prof. Arkady Major for giving me the opportunity to work in his research group. I deeply appreciate his continuous support of my M.Sc study and research, for his patience, guidance and immense knowledge.

I would also like to thank the members of my M.Sc. committee, Prof. Sherif Sherif and Prof. Gerald Gwinner for taking the time to review my thesis, participate in my defense and for their comments and suggestions.

I am grateful to all of my friends with whom I have had the pleasure to work during my project. Mohammad Nadimi, Chinedu Onyenekwu, Md. Anisur Rahman Reza, Chandan Qumar Howlader, Reza Akbari, Vladimir Montero Collado and Rubel Chandra Talukder. I really enjoyed by working in this group with such a wonderful environment.

Thanks also to my family: my parents Bemani Derakhshan, Mohammad Sedaghati, my sister Zahra Sedaghati and my brother Hossein Sedaghati for all their encouragement and motivation. Last but not least I would like to thank my loving husband who has provided unending inspiration, enthusiasm and support.

Table of Contents

List of Figures

List of Tables

List of symbols and abbreviations

Symbols (in order of appearance)

dn/dT	Thermo-optic coefficient
k_c	Thermal conductivity
n	Refractive index
h	Planck constant
ν_{pump}	Pump frequency
ν_{laser}	Laser frequency
P_{out}	Output power
P_{abs}	Absorbed pump power
P_{th}	Threshold pump power
η	Slope efficiency
L_i	Internal cavity loss
cw	continues wave
σ	Emission cross-section
τ	Upper state lifetime
λ_P	Pump wavelength
λ_L	Laser wavelength
M^2	Beam quality factor
M	Thermal lensing sensitivity factor
w_p	Pump radius
D	Dioptric power of thermal lens
Δ	Generalized thermo-optic coefficient
η_h	Fractional heat load
P_{PE}	Photo-elastic effect
$Q_{bulging}$	Bulging effect

Abbreviations

BRF	Birefringent filter
CW	Continuous-wave
FWHM	Full width at half maximum
HR	High-reflectivity
LD	Laser diode
DM	Dichroic mirror
DPSSL	Diode-pumped solid-state laser
NA	Numerical aperture
Nd	Neodymium
OC	Output coupler
QD	Quantum defect

Chapter 1: Introduction

1.1 Motivation

Nowadays, lasers (Light Amplification by Stimulated Emission of Radiation) have many applications in different areas such as medicine, industry, communications, etc [1]. T. Maiman introduced the first laser in 1960 [2], in which the gain medium was a ruby crystal (solid-state), and it was pumped with a flash lamp. Over the past 59 years, various classes of gain media such as solid-state, gas, liquid and semiconductor with different pumping approaches were developed [3]. Among them, diode-end-pumped solid-state lasers can offer high efficiency, excellent beam quality and high output power which are in high demand for many applications such as micromachining. However, achieving high power operation together with high efficiency and good output beam quality is a challenging task owing to the increased influence of thermo-optical effects which often lead to the degradation of laser performance.

Among the Nd-doped solid-state crystals operating in the near infrared range (such as YAG, KGW, glass, YVO_4, GVO_4 and YLF), the crystal of yttrium lithium fluoride (Nd:YLF) is an interesting one. This crystal was first developed in 1969 and has the benefits of natural birefringence (generates highly polarized laser beam), negative dn/dT (reduces thermal lensing effect) and long upper laser level lifetime (in favor of Q-switched lasers with high pulse energy). The emission spectrum of Nd:YLF has two main emission lines at 1047 nm (π-polarization) and 1053 nm (σ-polarization) [3].

To achieve a higher output power and/or higher efficiency, the losses of the laser system should be minimized. One of the mechanisms which contributes to this parameter is the quantum defect (the energy difference between the pump and laser photons). Therefore, reduction of the quantum

defect is an important factor for power scaling of the Nd:YLF lasers. This can be achieved by pumping the laser crystal at the absorption lines with longer wavelengths (such as 863, 873 and 881 nm) [4-6] than the traditional ~800 nm [7-10]. However, 881 nm is not the longest available absorption band for the Nd:YLF laser crystal. Recently, efficient diode-end-pumping around ~910 nm was realized for Nd:YVO_4, Nd:KGW and Nd:$GdVO_4$ lasers [11-14] which resulted in a lower thermal lensing effect [15,16] and increased efficiency [17-20]. In this work we used a similar approach and examined the performance of a continuous-wave Nd:YLF laser at 1047 nm under the 908 nm diode pumping.

1.2 Objectives

The traditional pumping approach of Nd:YLF is at ~800 nm. The purpose of this research was to explore the performance of a continuous-wave Nd:YLF laser at 1047 nm under a new in-band diode-pumping approach at 908 nm. The latter approach was expected to reduce the quantum defect by more than 50%. This, theoretically, should reduce the thermal lensing effect and enable efficient and high-power operation. Therefore, the main goals of this study were to:

- Experimentally investigate the performance of a continuous-wave 1047 nm Nd:YLF laser with in-band diode pumping at 908 nm.
- Study the thermal lensing effect of a 1047 nm Nd:YLF laser under 908 nm pumping and compare it with the traditional pumping wavelength at ~800 nm.
- Study the feasibility of the continuous-wave operation of a Nd:YLF laser at its second main emission line at 1053 nm under 908 nm pumping.

1.3 Contributions

The following contributions have been made in this thesis:

A continuous-wave operation of a Nd:YLF laser at 1047 nm with high efficiency and reduced thermal lensing effect under in-band diode pumping at 908 nm was demonstrated. A slope efficiency as high as ~73.9% was achieved. To the best of our knowledge, this is the first time that the performance of a Nd:YLF laser was investigated using the in-band pumping approach at 908 nm. The results of this work were presented at the Photonics North 2018 conference [21], Photonics West 2019 conference [22], and was submitted as a journal publication [23].

1.4 Outline of the thesis

This thesis consists of 4 Chapters.

Chapter 1 discusses motivation, objectives and contributions of the thesis.

Chapter 2 covers the background information related to this work. First, the important properties of Nd:YLF crystal are described. Then, the theory of the thermal lensing effect is introduced and the effect of the quantum defect on the reduction of the thermal lensing is discussed. At the end a review of previous work is presented.

Chapter 3 presents the experimental configurations and results. First, the cavity design is discussed and then the performance of a continuous-wave Nd:YLF laser at 1047 nm under in-band diode pumping at 908 nm is investigated. Then, the thermal lensing results are presented, and using numerical calculations are compared with previous work. The last part of this chapter discusses the preliminary results of 1053 nm Nd:YLF laser using the same in-band diode pumping approach.

Chapter 4 presents the conclusions and a brief overview on possible future work.

Chapter 2: Background information

In chapter 1 it was mentioned that efficient and high power operation of diode-pumped solid-state lasers is usually limited by the thermal lensing effect. Thermal lensing decreases the stability of the laser system and degrades the laser output beam quality. In extreme cases, it can also cause mechanical failure of the crystal. This chapter reviews the background of the relevant research, discusses the theory of the thermal lensing effect and highlights several previous relevant studies of Nd:YLF lasers with laser diode by pumping at different wavelengths.

2.1 Thermal lensing theory

Solid-state lasers, while operating, dissipate a certain amount of heat. The sources of this heat are various. However, they are mainly due to the energy difference between the pump band and the higher laser level as well as the energy difference between the lower laser level and the ground state [3]. The energy differences between the pump photons ($E_{Pump}= h\nu_{Pump}$) and the laser photons ($E_{Laser}= h\nu_{Laser}$) are known as quantum defect and can be expressed as

$$QD= h\nu_{Pump}- h\nu_{Laser}, \tag{2.1}$$

or can also be presented as the fraction of pump photon energy that is dissipated as heat

$$QD'= (1- \lambda_{Pump}/\lambda_{Laser})\times 100\%. \tag{2.2}$$

Figure 2.1 shows a schematic diagram of the quantum defect of a four-level laser system. It should be noted that Nd:YLF is known as a four-level system where the ground energy level and the lower laser energy level are well separated.

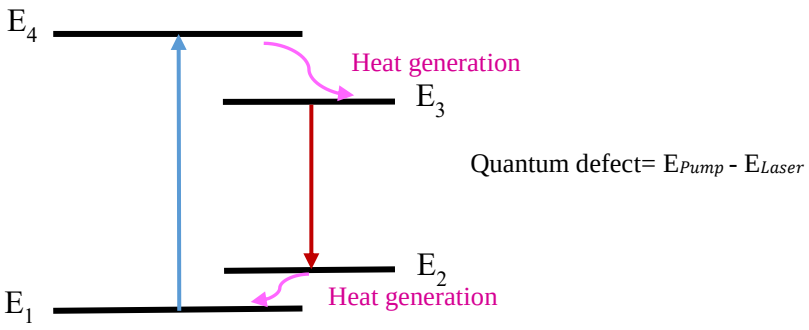

Figure 2.1- Schematic diagram of the quantum defect in a four-level laser system.

The generated heat causes temperature gradients inside the gain medium. The temperature gradient causes changes in the refractive index (*n*) of the crystal through a couple of main mechanisms including the thermo-optic effect which can be quantified by the material thermo-optic coefficient (*dn/dT*) and the photo-elastic effect which can be described as the changes in refractive index due to thermally induced mechanical stress. In addition, the thermally induced mechanical stress can cause the bulging of the end faces of the crystal.

The refractive index changes of the gain medium due to the thermo-optic and thermo-mechanical effects, together with end face bulging result in optical beam distortions within the crystal. These phenomena together can be usually modeled as a virtual thin lens within the gain medium. Therefore, this effect is well-known as the "thermal lensing" effect. Figure 2.2 shows the schematic diagram of the thermal lensing effect.

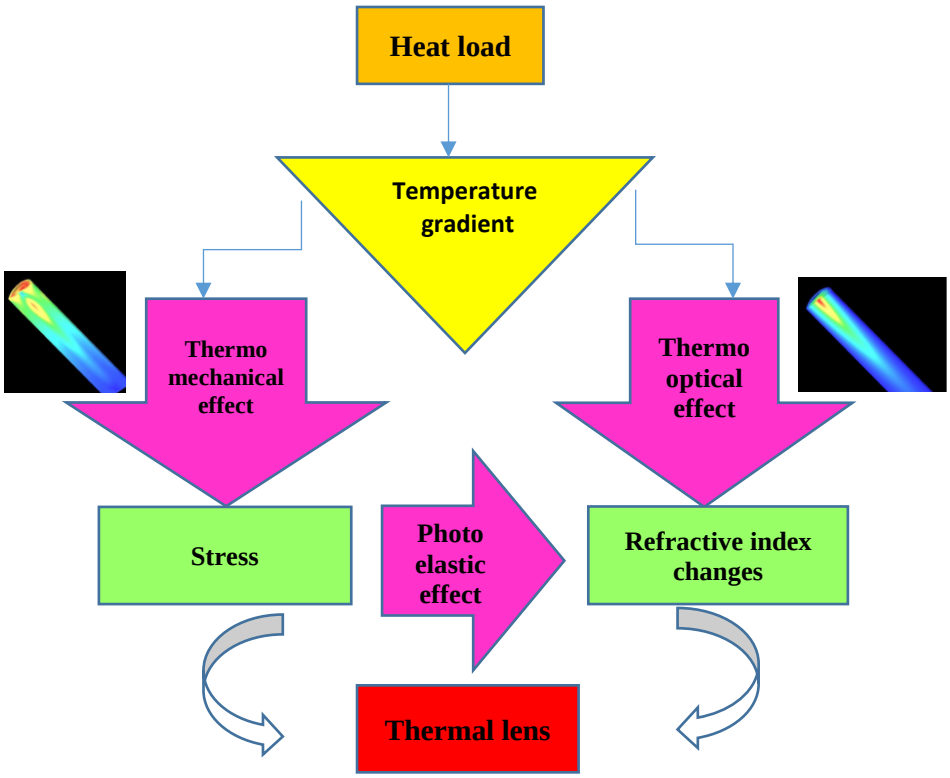

Figure 2.2- Schematic diagram of the nature of thermal lensing effect.

2.2 Nd:YLF laser crystal

2.2.1 Crystal structure, physical and thermoptical properties of Nd:YLF

Generally, active laser media are made of a host and dopants. Dopants typically are rare earth metal ions (Nd^{3+}, Er^{3+}, Yb^{3+}, …) or transition metals (Cr^{3+}, Cr^{4+}, Ti^{3+}, …). A combination of host material with the right concentration of dopant creates a laser gain medium which can possess favorable optical criteria. Dopants define the absorption and emission spectral characteristics of the lasing medium while the host determines material characteristics such as thermal conductivity and the refractive index.

The gain medium in this work consists of neodymium ions as dopant embedded in yttrium lithium tetrafluoride as host material which is usually expressed as $Nd:LiYF_4$ or Nd:YLF.

Nd:YLF has a tetragonal structure and is uniaxial. Its lattice parameters are $a=b=4.9589$ *Å* and $c=10.5050$ *Å*. Nd:YLF is a birefringent crystal and it has two major emission lines around 1050 nm; one located at 1047 nm for π-polarization (the electric field parallel to the optic axis (*c*-axis): $E \| c$, *a*-cut crystal) and the other one located at 1053 nm (the electric field perpendicular to the optic axis (*c*-axis): $E \perp c$, *a*- or *c*-cut crystals) for σ-polarization. Nd:YLF crystal has one optical axis. Optical axis is the direction in the crystal that allows any light passing through it to have the same speed as well as the same refractive index. If the electric field of propagating light is perpendicular to the optical axis of the crystal it is known as an ordinary wave (the related refractive index is called n_o). Whereas, when the electric field is parallel to the optical axis, it is known as an extraordinary wave (the related refractive index is called n_e). Birefringence is the difference between the n_e and n_o, $\Delta n = n_e - n_o$.

The birefringent characteristic of Nd:YLF can be explained by its anisotropic structure. It should be noted that crystals can be classified into two main groups (i.e. isotropic and anisotropic) based on their optical behavior and their crystallographic axes. The isotropic crystals have equal index of refraction in all directions. This causes similar behavior of light propagating inside the crystal despite the crystal orientation with respect to the incident light wave. When light enters an isotopic crystal, it refracts at a constant angle and passes within the crystal at a single velocity.

Unlike the isotropic crystals, anisotropic crystals have non-uniform properties and non-equivalent crystallographic axes. So, when the light propagates within anisotropic crystal, the characteristics of refracted light depends on the orientation of the crystalline lattice with respect to the angle of the incident light. Indeed, light exhibits different behaviors in an anisotropic crystal when it enters either parallel or perpendicular to the direction of the optical axis. When light enters along the optical axis of anisotropic crystals, it behaves like an isotropic crystal. On the other hand, when

light enters through a non-equivalent axis, it will be refracted into two polarized rays (with perpendicular to each other polarizations) and each of them will travel at a different velocity. This phenomenon is called birefringence or double refraction [24].

Table 2.1 lists the important characteristics of Nd:YLF crystal and compares them with the other two famous Nd-doped solid-state crystals, Nd:YAG and Nd:YVO_4. The main lasing wavelengths of Nd:YLF are at 1047/1053 nm and slightly lower than 1064 nm corresponding to the Nd:YAG and Nd:YVO_4. Nd:YLF and Nd:YVO_4 are uniaxial and can emit naturally polarized light and both belong to the tetragonal crystal lattice. In the tetragonal crystal structure of Nd:YLF and Nd:YVO_4, the two crystallographic directions indicate the same features (*a*-axis) and differ from the third direction (*c*-axis). Therefore, values for the index of refraction, thermal conductivity, thermo-optical coefficient and thermal expansion coefficient can be different along the a-axis and c-axis. Whereas, under the cubic structure of Nd:YAG, material properties are similar within the three crystallographic directions. The indices of refraction of Nd:YLF for both *a*- and *c*-axis directions are lower than those of the Nd:YAG and Nd:YVO_4. Nd:YLF has slightly higher thermal conductivity than Nd:YVO_4 and lower than Nd:YAG.

Nd:YLF offers longer upper state lifetime as compared to the other two crystals. This characteristic is in favor of lower threshold in CW lasers as well as high pulse energy in diode-pumped Q-switch lasers.

The thermo-optical coefficient of Nd:YLF (*dn/dT*) is negative and its magnitude is much lower than in Nd:YAG and Nd:YVO_4. This characteristic can cause a weaker thermal lensing effects for the Nd:YLF crystal compared to the other two crystals. The thermal expansion value of Nd:YAG is the same as Nd:YLF along the *c*-axis, whereas this value along the *a*-axis is larger than for Nd:YVO_4.

Table 2.1- A comparison of physical properties of Nd:YLF with Nd:YAG and Nd:YVO_4 [3,25-27].

Material / Property	**Nd:YLF**	**Nd:YAG**	**Nd:YVO_4**
Main lasing wavelength (nm)	1047 (π) 1053 (σ)	1064	1064 (π)
Crystal structure	tetragonal	cubic	tetragonal
Index of refraction (λ ~1.06 µm)	n_o=1.4481 (*c*) n_e=1.4704 (*a*)	1.82	n_e = 2.168 (*c*) n_o = 1.958 (*a*)
Thermal conductivity k_c [WK^{-1} m^{-1}]	5.8 (*c*) 7.2 (*a*)	12	5.23 (*c*) 5.1 (*a*)
Upper state lifetime τ_{21} [µs]	480	230	90
Thermo-optical coefficient dn / dT [K^{-1}]	-4.3×10^{-6} (*c*) -2.0×10^{-6} (*a*)	7.3×10^{-6}	8.41×10^{-6} (*c*) 15.5×10^{-6} (*a*)
Thermal expansion coefficient α_{th} [K^{-1}]	8×10^{-6} (*c*) 13×10^{-6} (*a*)	~ 8×10^{-6}	11×10^{-6} (*c*) 4.4×10^{-6} (*a*)

2.2.2 Spectroscopic properties of Nd:YLF

The absorption spectrum of Nd:YLF crystal is shown in figure 2.3. Its high absorption peaks are located within the 780-815 nm and 855-885 nm bands. It has been common to pump at 792 nm as it has the highest absorption peak for both polarizations.

It should be noted that the traditional pumping wavelength for Nd:YLF is at ~800 nm and the longest pumping wavelength that has been reported to date was at ~880 nm [28,29]. As it is shown in figure 2.3, there are some small absorption peaks available at ~908 nm that may be used for pumping and to the best of our knowledge have not been studied so far for Nd:YLF. Indeed, laser operation with a pump wavelength around 912 nm has been previously reported for other Nd-doped crystals like Nd:YVO_4, Nd:KGW and Nd:$GdVO_4$ [11-14,16-17,30]. In this work, we

investigated pumping of the Nd:YLF laser crystal at 908 nm.

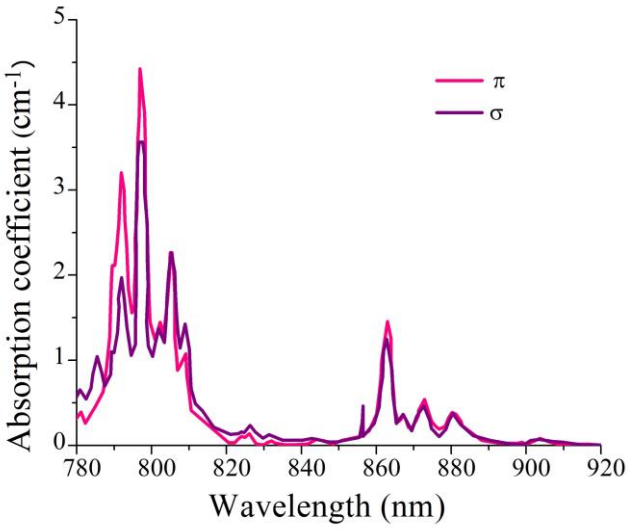

Figure 2.3- Absorption spectrum of the Nd:YLF [31].

The emission spectrum for an *a*-cut Nd:YLF crystal is shown in figure 2.4. The main emission lines are at 1047 nm (π- polarization) and 1053 nm (σ-polarization). The secondary emission lines are also available at 1042, 1057 and 1072 nm for the π-polarization and at 1042, 1047, 1067 and 1074 nm for the σ-polarization [32] that can be utilized by suppression of the main emission lines.

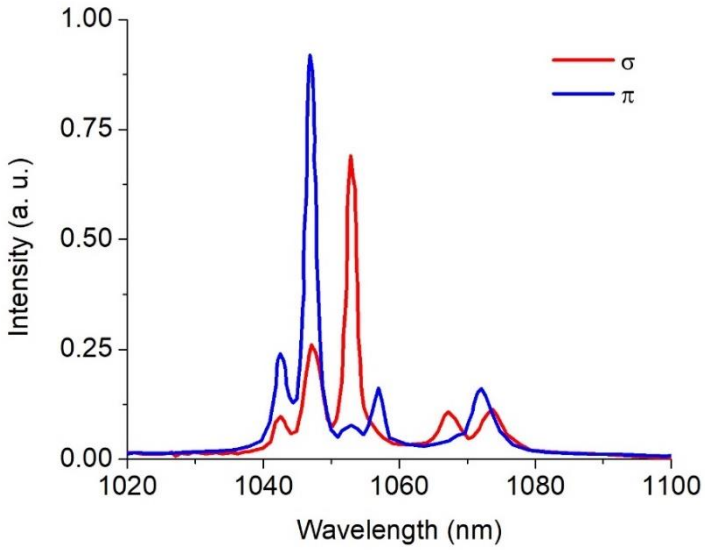

Figure 2.4- Emission spectrum of an *a*-cut Nd:YLF crystal in π- and σ-polarizations under 803 nm excitation [32].

The geometry of the *a*-cut Nd:YLF crystal used in the study is demonstrated in figure 2.5. It should be noted that an *a*-cut Nd:YLF crystal is attractive owing to its superior absorption and emission spectral features rather than *c*-cut.

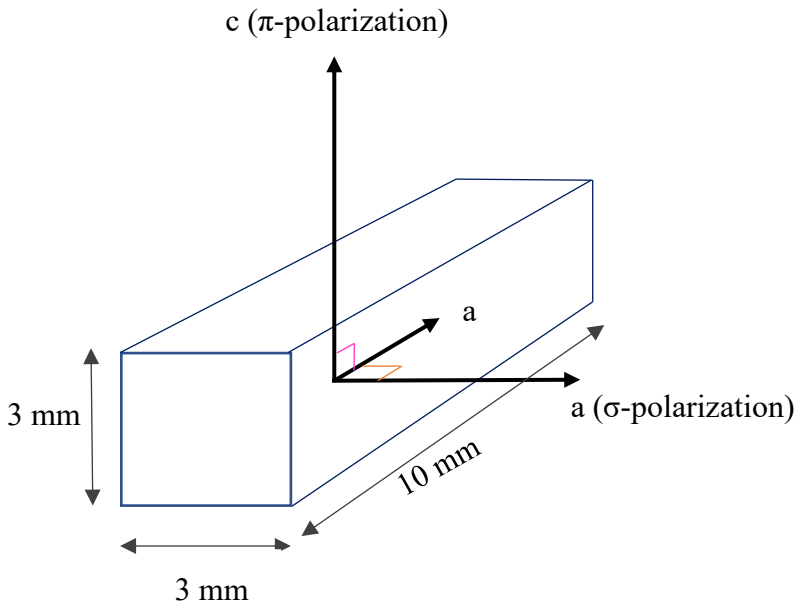

Figure 2.5- The Nd:YLF crystal geometry used in this work.

2.3 Pumping at 908 nm

2.3.1 Low quantum defect pumping

As discussed in section 2.1, the reduction of the quantum defect can generate less heat in the gain medium and therefore reduce the thermal lensing effect and indeed scale the maximum achievable output power of the laser system. One strategy to reduce the quantum defect in diode-pumped solid-state lasers is direct pumping [33]. The idea of direct pumping is to promote the laser operation by pumping Nd^{+3} ions directly to a higher upper level or by pumping the laser crystal at a longer wavelength. Considering equation 2.2, if the pumping wavelength gets closer to the lasing wavelength, the quantum defect (and thermal lensing) will decrease.

Pumping at long wavelengths such as 863, 873 and 881 nm were previously reported for Nd:YLF laser [4-6] and higher laser efficiency was reported in comparison with traditional pumping at ~800 nm.

Figure 2.6 shows the schematic of the energy band diagram for pumping Nd:YLF at different wavelengths. It can be seen that as the pumping wavelength increases, the energy difference between the pump and laser photons decreases (compare with figure 2.1). The pump wavelength of 908 nm (which was used in this work) reduces the quantum defect by more than 50% when compared to the conventional pumping around 800 nm. Hence, in-band direct diode pumping (pumping the laser active ions directly into the upper energy level of the laser transition) at ~908 nm for Nd:YLF crystal should reduce the thermal lensing effect and therefore may open a pathway to power scale the laser output.

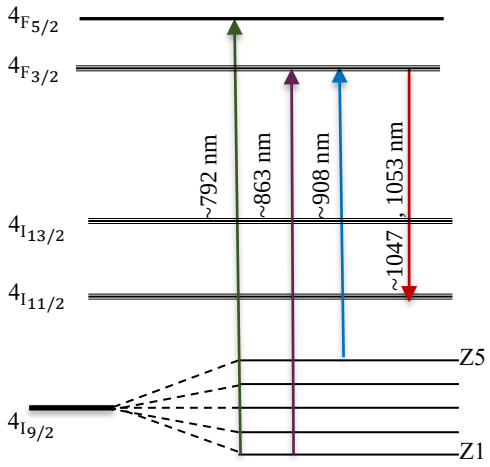

Figure 2.6- Energy levels of the Nd:YLF crystal.

2.3.2 High slope efficiency

Equation 2.3 can be used to analyze and study the relation between the pump wavelength and the slope efficiency on the output of the CW laser [34,35]:

$$P_{out} = \frac{-\ln(1-\mathrm{T})}{\ln(1-\mathrm{T})+\mathrm{Li}} \times \frac{\nu_{\mathrm{Laser}}}{\nu_{\mathrm{Pump}}} \times (\mathrm{P_{abs}} - \mathrm{P_{th}}), \tag{2.3}$$

where P_{out} is the output power, P_{abs} is the absorbed pump power and P_{th} is the threshold power. T is the transmission corresponding to the output coupler, L_i is the internal cavity loss.

It is also possible to replace the v_{Laser} with the wavelength in this equation. Equation 2.4 will be obtained based on the pump wavelength as

$$P_{out} = \frac{-\ln(1-\mathrm{T})}{\ln(1-\mathrm{T})+\mathrm{Li}} \times \frac{\lambda_{\mathrm{Pump}}}{\lambda_{\mathrm{Laser}}} \times (P_{\mathrm{abs}} - P_{\mathrm{th}}). \tag{2.4}$$

The slope efficiency for a CW laser (η) based on equation 2.4 can be defined as [17]

$$\eta = \frac{-\ln(1-\mathrm{T})}{-\ln(1-\mathrm{T})+\mathrm{L}_i} \times \frac{\lambda_{\mathrm{Pump}}}{\lambda_{\mathrm{Laser}}}\,. \tag{2.5}$$

According to equation 2.5, as the pumping wavelength increases and gets closer to the laser wavelength, the slope efficiency is expected to increase. Therefore, longer wavelength pumping at 908 nm should lead to a higher slope efficiency compared to the traditional pumping at 800 nm.

Equation 2.6 presents the threshold pump power for the CW laser by assuming that it has the best mode matching between the laser mode and the pump mode [34,35]:

$$\mathrm{P_{th}} = \frac{\pi h \nu_{Pump} w^2 (\mathrm{L}_i - \ln(1-\mathrm{T}))}{2\sigma\tau}\,, \tag{2.6}$$

where h is Planck's constant, w is the beam waist for the pump, σ is the emission cross-section and τ is the upper state lifetime. As the pumping wavelength increases, the pump photon energy

decreases and the threshold pump power for the CW laser becomes laser. This is an additional benefit of low quantum defect pumping at longer wavelength.

2.4 Previous results

2.4.1 Previous records of Nd:YLF laser in-band pumped at 808 nm

In this section, some of the previous reports of Nd:YLF laser are discussed.

In 2010, Yan-Fei Lü et al. studied the performance of a 1047 nm Nd:YLF laser using a Ti:Sapphire laser as a pump source [5]. The gain medium was 3×3×8 mm^3, *a*-cut with 1.0-at.% doping (at.% or atomic percent is the percentage of one kind of atom relative to the total number of atoms). Figure 2.7 shows the related setup which included a cavity with two mirrors, where mirror M1 had a high reflection (HR) coating at 1047 nm (R > 99.9%) and a high transmission coating at the pump wavelength (T > 99%). Mirror M2 was plano-concave with 200 mm radius of curvature and had 10% transmission at 1047 nm. Also, a Brewster plate was used in the cavity to create additional loss for the σ-polarization (to have a stable single line of 1047 nm).

The Nd:YLF laser was pumped at 806 nm, 863 nm, 872 nm and 880 nm wavelengths. The slope efficiencies with respect to the absorbed pump power were reported to be 55.6%, 65.1%, 71.2% and 76.3%, respectively, while the output powers were between 0.8 to 1.05 W. It should be noted that the Ti:sapphire laser pump itself needs another pumping source and therefore the overall system was complex, very costly and not efficient. Better efficiencies observed at longer wavelengths are in agreement with our discussion in section 2.3.2.

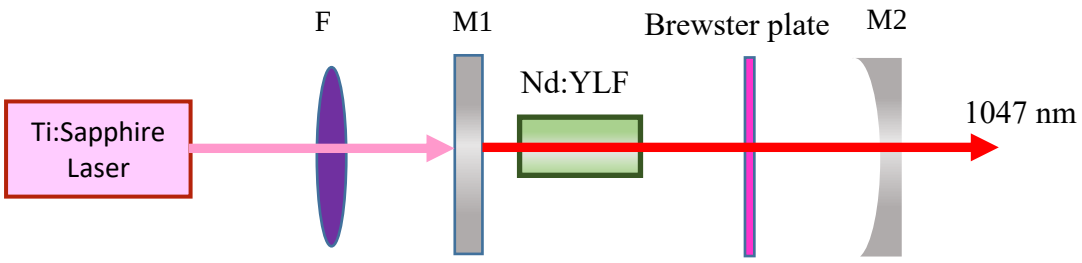

Figure 2.7- Schematic setup of Nd:YLF laser [5]. M1: flat dichroic mirror, M2: concave mirror (OC). Brewster plate is for additional loss for 1053nm to have a single line of 1047 nm.

In another interesting work, a Nd:YLF crystal was pumped with an end pumped fiber-coupled diode laser at ~803 nm by Zhi Lin et al, in 2015 [32]. The gain medium was 1 at. % Nd:YLF crystal, *a*-cut with the dimension of 3×3×4 mm³. The cavity had 2 mirrors (figure 2.8). M1 was a flat dichroic mirror with a maximum transmission (T~90%) at the pump wavelength and high reflectivity (R>99.9%) around 1053 nm. Mirror M2 was plano-concave and was used as an output coupler with the radius of curvature of 1000 mm (~6.5% transmission at 1047nm and ~6.1% at 1053 nm).

The authors reported a laser transition from the single wavelength operation at 1047 nm to the dual-wavelength operation at the 1047-1053 nm pair or to the single wavelength operation at 1053 nm. One of the main reasons for such a transition was believed to be the higher loss of the π-polarized 1047 nm laser radiation at high powers due to its stronger negative thermal lensing effect. In the gain competition between the 1047 nm and 1053 nm lines, this could let the latter oscillate even though it has a lower emission cross-section. As indicated in table 2.1, the *dn/dT* of the π- and σ-polarized laser emission for the Nd:YLF crystal is -4.3 and -2×10^{-6} K^{-1}, respectively [27,36]. Therefore, upon oscillation, it was expected for the 1053 nm laser line to have a weaker thermal lensing effect.

A single-wavelength laser emission at around 1047 nm was first observed at a laser threshold of ~0.5 W pump power. Afterward, the dual-wavelength laser at 1047 & 1053 nm was reported at a

pump power of 5.77 W with a maximum output power of ~1.25 W and slope efficiency of about 50.9%. By increasing the pump power to 15.34 W, a single-wavelength 1053 nm laser was achieved with a maximum output power of 3.36 W. Next, a glass etalon (0.1 mm) was added in the cavity to obtain a dual-wavelength laser operation at 1047 and 1072 nm.

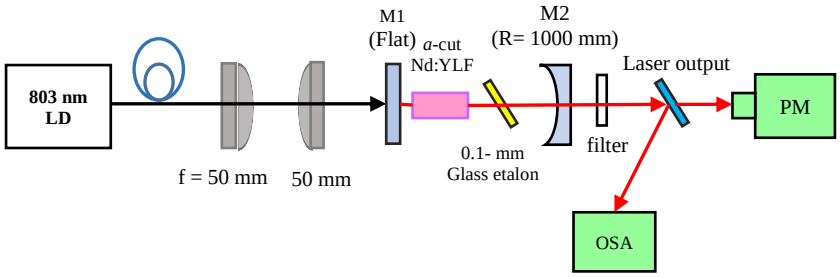

Figure 2.8- Schematic design setup of the Nd:YLF laser [32]. M1: flat dichroic mirror, M2: concave mirror (OC). Glass etalon: to achieve a dual-wavelength laser at 1047 and 1072 nm. PM: power meter, OSA: optical spectrum analyzer.

In 2017, El-Agmy et al. studied the effect of the laser crystal geometry on its temperature and stress distribution by using numerical modeling simulation. They explored the geometry effect on the Nd:YLF laser rod under 805 nm diode pumping [37]. The results of the finite element simulation showed a thinner rod would result in power scaling the output power by 50% before reaching the limits imposed by the thermal effects. Likewise, in the experimental work they applied 805 nm laser diode light to a laser rod of 10 mm length and 4 mm radius and 0.7-at.% Nd-doping. The cavity consisted of two mirrors. The authors used an HR mirror with ~99.5% reflection at 1053 nm wavelength and ~0.5% antireflection coating at 805 nm wavelength. By using a 5% transmission OC, the laser generated 7.2 W output power at 1047 nm under 30 W of pump power. Considering around 85% of absorption efficiency, the optical efficiency versus the absorbed pump power was ~28%. We believe that any optimization of the crystal geometry that was proposed for the traditional pumping wavelength can be applied to 908 nm pumping as well.

Very recently, Qinglei et al. reported a 13.6 W CW Nd:YLF laser operating at 1053 nm [38]. To

reduce the problem related to stress-induced fracture, they pumped at ~808 nm instead of ~797 nm. The crystal was an *a*-cut 0.5% doped rod, 35 mm long and with 3 mm radius. The cavity consisted of three mirrors and a fiber-coupled laser diode as a pump source. The pump was focused into the gain medium through a lens barrel system. Mirror M1 had 500 mm curvature with a HR coating at 1053 nm and an antireflection coating at 808 nm wavelength, M2 was with a 400 mm curvature and high reflection for 1053 nm wavelength. M3 was an OC with 15% of transmission. Furthermore, the Brewster plate in the cavity suppressed 1047 nm laser line in order to have only a single wavelength operation at 1053 nm.

The schematic of the experimental setup is shown in figure 2.9. In the CW regime, 13.5 W output power was obtained with a pump power of ~30 W. The optical-to-optical and the slope efficiency were 45% and 51%, respectively, while the beam quality factor M^2 was around 1.02 indicating a perfect Gaussian beam.

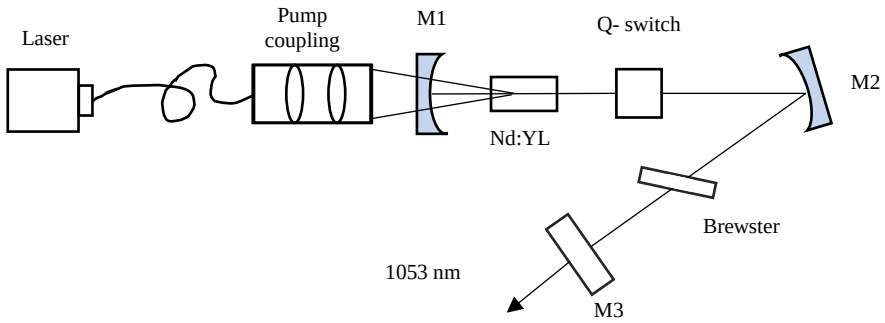

Figure 2.9- schematic design setup of Nd:YLF laser. M1 and M2 are curved mirror. M3 is the output coupler. Brewster plate was used suppress the 1047 nm laser.

Chapter 3: Experimental setup and results

As discussed in chapter 2, thermal lensing is the main limitation that can affect the laser output power as well as the thermal stability in a laser cavity, the slope efficiency, and the beam quality. In-band pumping with laser diode at 908 nm has an important role to reduce the thermal problems.

Also, in order to generate laser radiation with high efficiency and high beam quality, an appropriate optical resonator should be designed. For a proper cavity one needs to choose the distances between each optical element in a manner such that a good overlap between the pump beam and the laser cavity beam is achieved (also known as mode matching). Mode matching between the pump and laser beams is affected by the thermal lensing effect. Therefore, the thermal lensing effect also should be considered while deciding on the distances of the cavity lens/mirror system. This chapter presents the design and study of the performance of an efficient CW Nd:YLF laser and its thermal lensing effects under in-band diode pumping at ~908 nm.

3.1 Laser diode (pump source)

In chapter 2, it was discussed that in the present research Nd:YLF crystal would be diode pumped at ~908 nm. The pump system in this study was provided by a high power fiber-coupled laser diode which was operating in the 905-915 nm wavelength range. The fiber core diameter was 105 μm with a numerical aperture of 0.22. The maximum output power of the diode source that was used in this work was 42.7 W at 3.75 A, as shown in figure 3.1. By using a collimating (f=40 mm) lens and a focusing (f=200 mm) lens, the pump beam was focused into the center of the gain medium with a spot size radius of ~262.5 μm.

The laser diode had a spectral widths of ~3 nm (FWHM). The temperature of the laser diode was monitored using a built-in thermistor and it was set to operate at ~17.5 ˚C to let the central wavelength of the laser diode be ~908 nm. In order to calculate the absorbed pump power within the Nd:YLF crystal, the laser diode power was recorded before and after it passed through the crystal. The results are presented in figure 3.2. The nonlinear behavior of the absorbed power versus diode drive current is caused by the variation of the diode's central wavelength due to the temperature change.

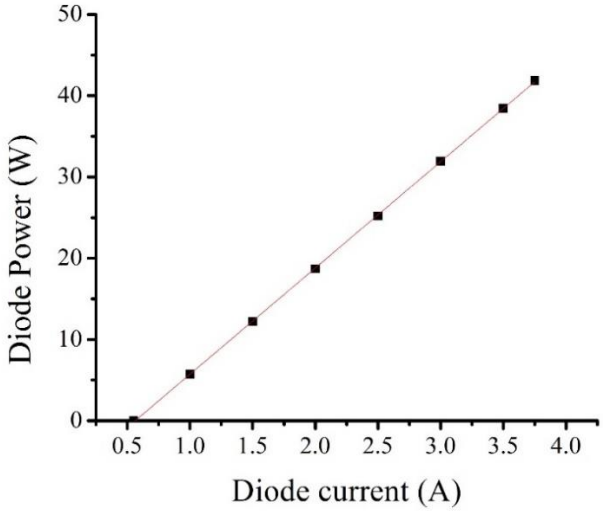

Figure 3.1- Laser diode pump output power vs. drive current.

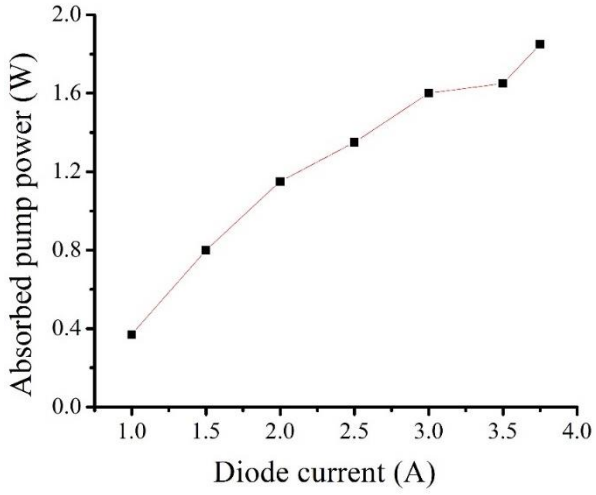

Figure 3.2- Absorbed pump power vs. laser diode drive current.

3.2 Laser cavity design

In a cavity design, a good overlap between the pump and laser beams is needed. The cavity can be designed using an ABCD matrix analysis technique where optical elements are characterized using 2×2 matrices (see appendix A). Therefore, by using the ABCD technique, it is possible to choose the appropriate distances between the elements in the cavity in a way that a reasonable mode matching is obtained. It should be noted that the cavity design is an iterative process and it doesn't have any unique solution.

In this work, the reZonator software [39] and the LASCAD software [40] were mainly used for modeling of the cavity and beam size analysis. In the laser cavity design process, we chose a three-mirror cavity. The effective thermal lens was modeled as a thin lens at the center of the laser crystal (as discussed in section 2.1). The schematics of the laser cavity in reZonator software is shown in figure 3.3. M1 is a plane mirror, L1, L2 and L3 are the propagation distances in free space, Cr1 and Cr2 are the two halves of the crystal. F1 is the effective thermal lens, M2 is the lens corresponding to the concave folding mirror and M3 is the output coupler (OC). Figure 3.4 shows the laser beam radius change along the length of the cavity as well as suitable mode matching between the laser beam size and the pump beam size (~262.5 μm) around 50 mm of distance.

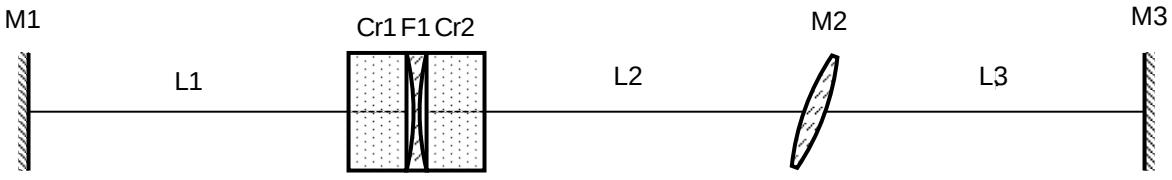

Figure 3.3- Schematic diagram of the laser cavity used in ABCD matrix calculation.

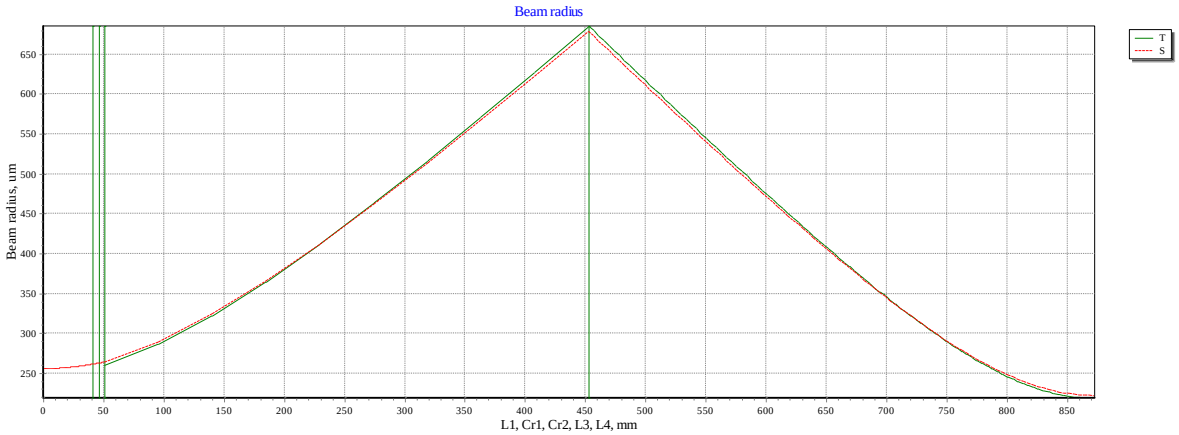

Figure 3.4- Beam radius inside a resonator (T denotes the tangential plane which is the horizontal plane containing elements of a resonator and S denotes the sagittal plane which is the vertical plane containing optical axes of the elements and it is normal to the tangential plane [39]).

3.3 Experimental set-up

3.3.1 Experimental set-up for CW laser operation at 1047 nm

Figure 3.5 shows the schematic of the continuous-wave (CW) laser experimental setup. The gain medium was an *a*-cut Nd:YLF crystal with dimensions of 3×3×10 mm^3 and 1-at.% doping concentration. The laser crystal was wrapped with indium foil and was water-cooled at 16 ℃ on its top and bottom surfaces. As mentioned in section 3.2 the laser cavity consisted of three mirrors, where M1 was a flat dichroic, M2 was a concave mirror (with 500 mm radius of curvature) and OC was a flat output coupler. The transmission of the output coupler was selected such that it provided the maximum output power. Three distinct output couplers with different transmission of 5%, 7.5% and 10% were tested and the highest output power was obtained with 7.5% transmission and it was kept in the cavity for the rest of the experiment. The distances L1, L2 and L3 were 4.1, 40.2 and 43 cm, respectively. The pumping system (as discussed in section 3.1) was a fiber-coupled laser diode operating around 908 nm (105 μm core diameter, NA= 0.22). The pumping beam was focused into the middle of the laser crystal and created a pump spot size of ~262.5 μm radius.

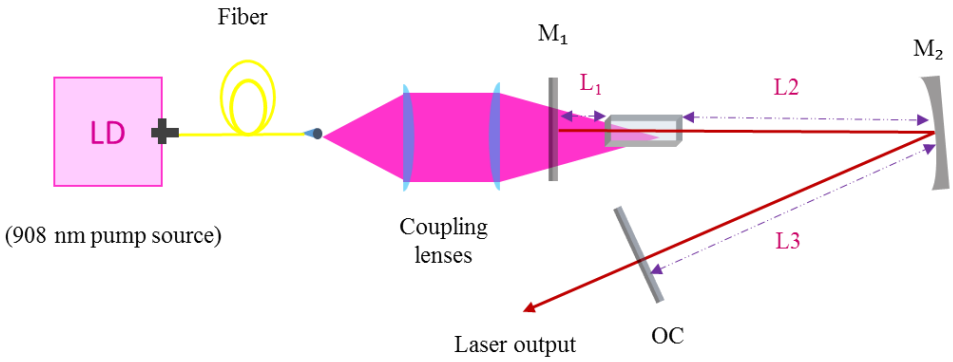

Figure 3.5- Experimental setup for continuous wave operation.

3.3.2 Experimental set-up for thermal lensing measurement at 1047 nm

The goal of this section was to measure the focal length of the induced thermal lens inside the gain medium. To measure the created thermal lensing strength, a modified ABCD-matrix beam propagation technique was used to measure the sign and magnitude of the thermal lensing effect [16,41] The thermal lensing measurement set-up is shown in figure 3.6 which is similar to the figure of 3.5. Indeed, outside the cavity, the beam widths in vertical and horizontal directions of the laser output beam were recorded after a focusing lens. It should be noted that the second dichroic mirror (DM) was used in the setup to remove the residual pump power. The beam profiler was located at different distances from the lens in order to measure the beam characteristics.

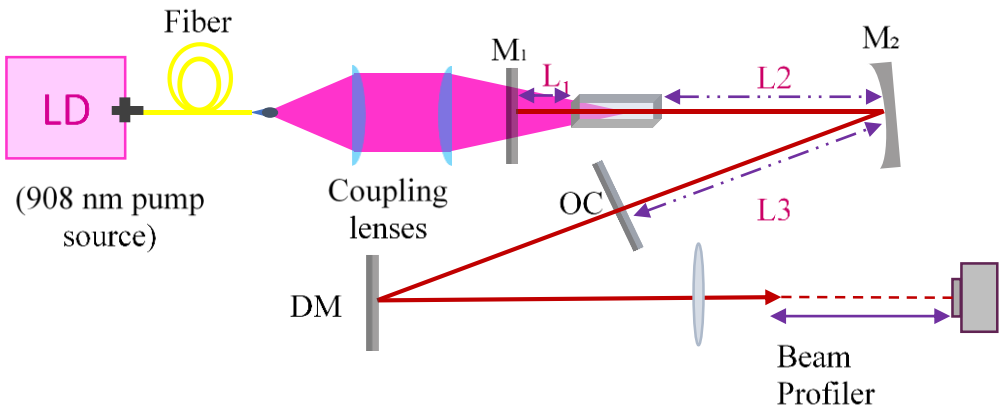

Figure 3.6- Experimental setup for thermal lensing measurement.

The laser beam quality factor (M^2) represents the deviation of a beam from an ideal Gaussian beam for which M^2=1. The M^2 and the laser beam waist, ω_0, can be estimated by fitting the recorded laser beam width data to the Gaussian propagation equation using equation 3.1 [41],

$$\omega(z) = \omega_0 \left[1 + \left(\frac{M^2 \lambda_0 z}{n \pi \omega_0^2}\right)^2\right]^{1/2} \quad (3.1)$$

in which λ_0 is the output laser wavelength, n is the refractive index and z is the distance from the beam waist along the beam propagation direction.

The methodology that a modified ABCD-matrix beam propagation technique uses to find the thermal lensing focal lens is based on the concept that the thermal lens can be modeled as a virtual lens inside the crystal. The laser cavity should be simulated in software with a variable lens at the center of the gain medium. The experimentally measured output beam waist radius should be recorded. The focal length of the virtual lens should then be adjusted to obtain the simulated output beam characteristics similar to the experimentally measured value. The M^2 used in the simulation should be the same as the experimental value.

The commercial LASCAD software was used in our work to simulate the beam propagation. Figure 3.7 shows the equivalent laser cavity and the laser beam propagation.

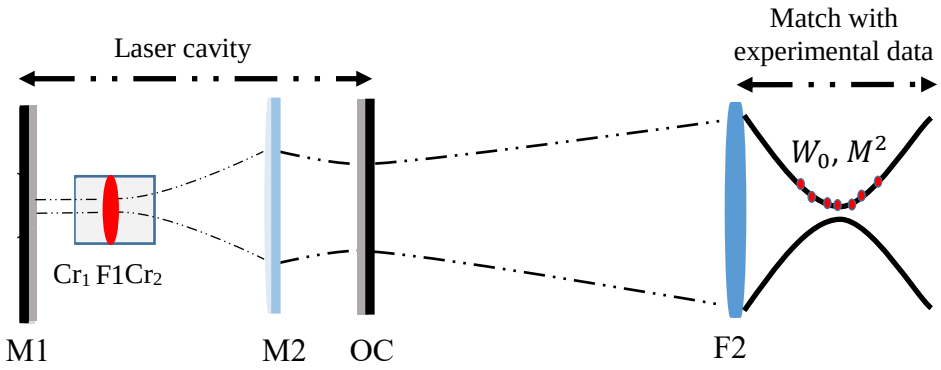

Figure 3.7- The laser cavity used in the LASCAD software.

3.4 Experimental results at 1047 nm

3.4.1 Experimental results on CW laser operation at 1047 nm

Figure 3.8 illustrates the measurement results of the output power for the 1047 nm CW Nd:YLF laser versus the absorbed pump power using three different output couplers. The laser achieved maximum output power of 850 mW under 42 W of pump power (1.85 W absorbed pump power). The maximum slope efficiency of ~73.9% versus the absorbed pump power was achieved with a 7.5% output coupler. The lower slope in the low power regime (<250mW) may be explained by the wavelength shift of the laser diode as the pump power was increased. The incident pump power absorption efficiency was ~4.5% which limited the absorbed pump power to 1.85W. Such a low value of absorption can be offset in future experiments by using a longer crystal or higher doping concentration.

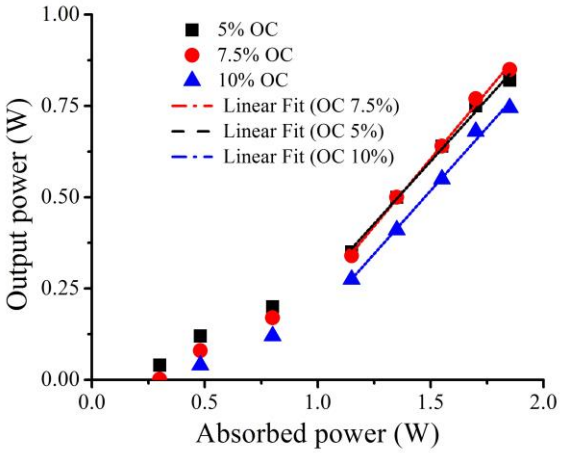

Figure 3.8- Output power versus the absorbed pump power.

The laser produced a good output beam shape with a high beam quality. The beam quality factor (M^2) was found to be around 1.36 at full power operation. The measured beam shape, beam radii and the beam quality factors are presented in figure 3.9.

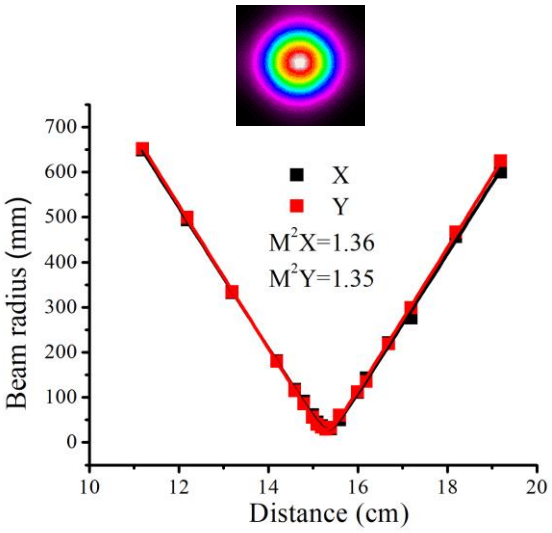

Figure 3.9- Laser beam quality measurement at 850 mW of output power. Inset**:** output beam shape.

The spectrum of the laser output is shown in figure 3.10. The peak value of the spectrum was at 1046.9 nm with the linewidth at half-maximum measured to be around ~0.1 nm which was limited by the resolution of the used spectrometer (Anritsu MS9710B). The output laser radiation was vertically polarized (*E* // *c*-axis, π-polarized).

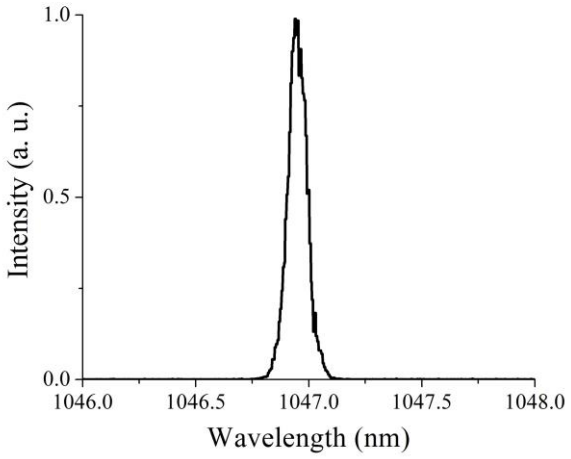

Figure 3.10- CW laser spectrum.

Improved efficiency for Nd:YLF crystal by long wavelength pumping methodology at 863 nm (side pumping) [42] and 880 nm (Ti:sapphire laser pumping) [5] were previously reported.

In the present work, we showed that 908 nm is another available absorption band for 1047 nm Nd:YLF laser. Although in our case the slope efficiency was a bit lower than with the Ti:sapphire laser pumping (73.9% vs 76.3%), we believe that it is the highest one for the directly diode-pumped Nd:YLF lasers. It should be noted that the Ti:sapphire laser itself makes the overall system complex, very costly and not efficient as it requires another laser pump source.

3.4.2 Thermal lensing results

In order to have a better idea of the thermal lensing strength of the demonstrated in-band diode-pumped Nd:YLF laser, we measured it using a modified ABCD-matrix analysis method [16,41] as described in section 3.2.1. At ~1.85 W of absorbed pump power, the focal length of the thermal lens was obtained to be -7290 and -2200 mm in the horizontal and vertical directions, respectively. The weak thermal lensing strength in the experiment supports the observed single wavelength

operation at 1047 nm. As we expected thermal lensing was stronger in the vertical direction due to the cooling direction of the crystal.

To validate the obtained thermal lensing results they were compared with the results from previous work. Using the numerical model described in [16], the thermal lensing strength can be predicted in various experimental settings provided that the thermal lensing sensitivity factor *M* would be available at one of the pump wavelengths. The thermal lensing sensitivity factor is defined as the slope of the thermal lensing dioptric power dependence on the absorbed pump power and can be written as [16]:

$$M=\frac{dD}{dP_{abs}}=\frac{n_h}{2k_c\pi w_p^2}\,\Delta\ , \tag{3.2}$$

where D is the thermal lensing dioptric power, P_{abs} is the absorbed pump power, ω_p is the pump waist radius, k_c is the thermal conductivity. The η_h is the fractional heat load (a fraction of the absorbed pump power that is dissipated as heat in the gain medium) which can be approximated as $1-\lambda_p/\lambda_l$, where λ_p and λ_l are the pump and laser wavelengths. Δ is the "generalized" thermo-optic coefficient which represents the three main mechanisms of thermal lensing effect known as thermo-optic effect (dn/dT), photo-elastic effect (P_{PE}) and crystal end face bulging effect ($Q_{bulging}$). It can be expressed as:

$$\Delta=\left(\frac{dn}{dT}+P_{PE}+Q_{bulging}\right). \tag{3.3}$$

Using the tabulated experimental data from [37] for a 0.7-at.% doped, 10-mm long, 4-mm diameter Nd:YLF rod, one can calculate the thermal lensing sensitivity factor to be ~-0.292 m^{-1}/W for the ω_p of 300 μm and at the pumping wavelength of 805 nm. The Δ can then be also calculated as -4.14×10^{-6} K^{-1}. Considering the value of the dn/dT of -4.3×10^{-6} K^{-1} for the π-polarized light

[27,36], the similarity in the calculated Δ and dn/dT values can be interpreted as the case when contributions of the bulging and photo-elastic effects are fairly small. From this experimental data, the dependence of the sensitivity factor on the pump beam waist radius ω_p at the pumping wavelengths of 805 nm and 908 nm was numerically calculated and is displayed in figure 3.11(a). This can be done because the "generalized" thermo-optic coefficient Δ is the same for the pumping wavelengths of 805 and 908 nm since it does not depend on the source of heat. Details of similar calculations can be found elsewhere [16]. Using our experimental conditions, the thermal lensing sensitivity factor for the ω_p of 262.5 μm and at the pump wavelength of 908 nm can thus be predicted to be -0.219 m^1/W (green square in figure 3.11(a)). This means that a 1 W increase in the absorbed pump power results in the 0.219 m^{-1} increase in the dioptric power of the induced thermal lens as shown in figure 3.11(b). Therefore, one should expect the thermal lensing power of -0.405 m^{-1} (focal length of -2468 mm) at 1.85 W of the absorbed pump power which is within 13% of our experimentally measured value of -0.45 m^{-1} (focal length of -2200 mm). This fact allows us to make a rough estimation of the sensitivity factor in our experimental conditions using only a single measurement of the thermal lens. Assuming that there is no lens at zero power and using the measured f=-2200 mm as a second data point, the *M* factor in our experiment can be evaluated as -0.246 m^{-1}/W which is fairly close to the one (-0.219 m^{-1}/W) calculated from the data of [37]. This approximate experimental value of the *M* factor is included in figure 3.11(a) as a purple dot.

This analysis shows that our thermal lensing data are very reasonable, and that thermal lensing is about twice weaker than that with 805 nm pumping. This low thermal lensing effect points to a new methodology for power scaling of Nd:YLF lasers and confirms the single wavelength operation at 1047 nm in our work.

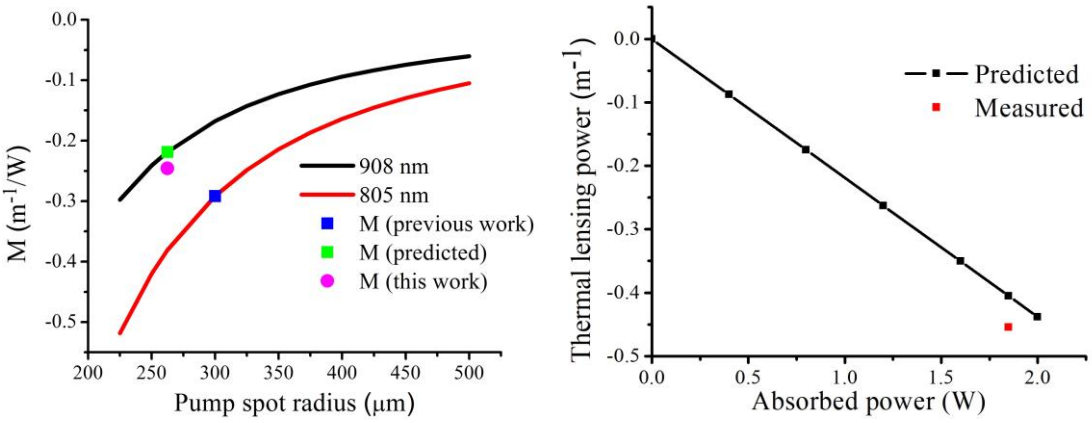

Figure 3.11- a) Thermal lensing sensitivity factors versus pump spot radius for the diode-pumped Nd:YLF lasers. Red and black curves: numerical calculation of *M* at various pump spot sizes with 805 and 908 nm pumping wavelengths, respectively. Blue square (lower curve): *M* measured under the 805 nm pumping [37]. Green square (upper curve): predicted value of *M* under the 908 nm pumping. Purple dot (upper curve): the measured value of *M* under the 908 nm pumping. b) Thermal lensing dioptric power versus the absorbed pump power under the 908 nm pumping and for the pump beam waist radius of 262.5 μm. Solid black line: predicted thermal lensing dioptric power based on the *M* of -0.219 m^{-1}/W. Red square: thermal lensing dioptric power measured in this work.

3.5 Nd:YLF laser performance at 1053 nm

As discussed in section 2.2.2, the second main emission line of Nd:YLF laser is located at 1053 nm. As a side work of the present research, we were interested to examine the possibility of the operation of Nd:YLF laser at 1053 nm under 908 nm pumping. To achieve that, the oscillation of the main emission band at 1047 nm should be suppressed. This can be done by implementing an additional intracavity loss element within the laser setup such as etalons and birefringent filters [20,43-44]. Indeed, we used a cavity similar to figure 3.5 and added a 2 mm-thick intracavity birefringent filter at the Brewster angle. The new setup up is shown in figure 3.12.

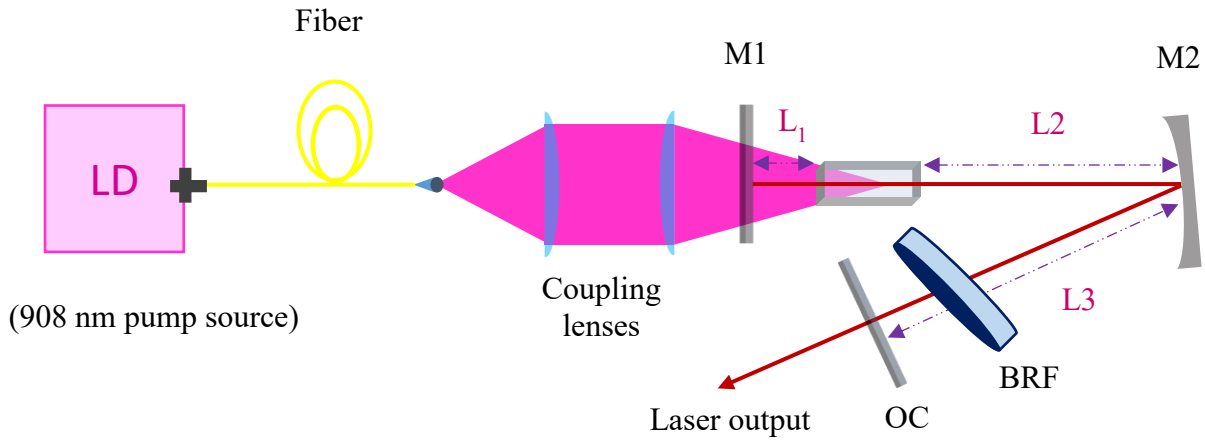

Figure 3.12- Experimental setup for CW operation.

The measurement results of laser output power at 1053 nm with respect to the absorbed pump power is shown in figure 3.13. The maximum laser output power reached 625 mW. The slope efficiency versus the absorbed pump power was ~46% and the optical efficiency was about ~34%.

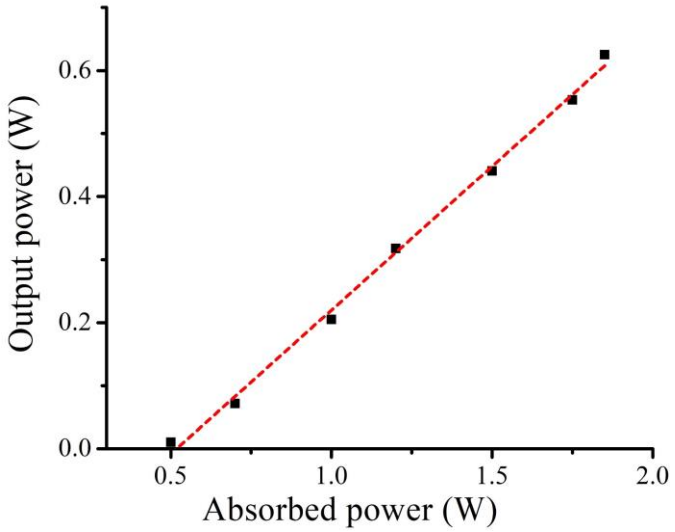

Figure 3.13- Output power versus the absorbed pump power.

The beam quality factor M^2 was found to be around 1.37 and 1.26 in the *x* (horizontal) and *y* (vertical) directions, respectively. The measured beam shape, beam radii and the beam quality factors are shown in figure 3.14

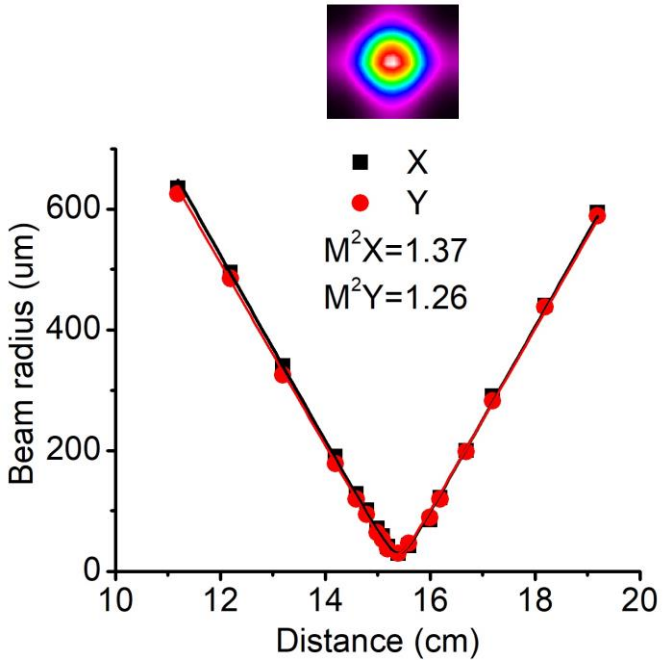

Figure 3.14- Laser beam quality measurement at 625 mW of output power. Inset**:** output beam shape.

The spectrum of the laser output is shown in figure 3.15. The peak value of the spectrum was at 1052.9 nm with the linewidth at half-maximum measured to be around ~0.1 nm and was limited by the resolution of the used spectrometer. The output laser radiation was horizontally polarized ($E \perp c$-axis, σ-polarized).

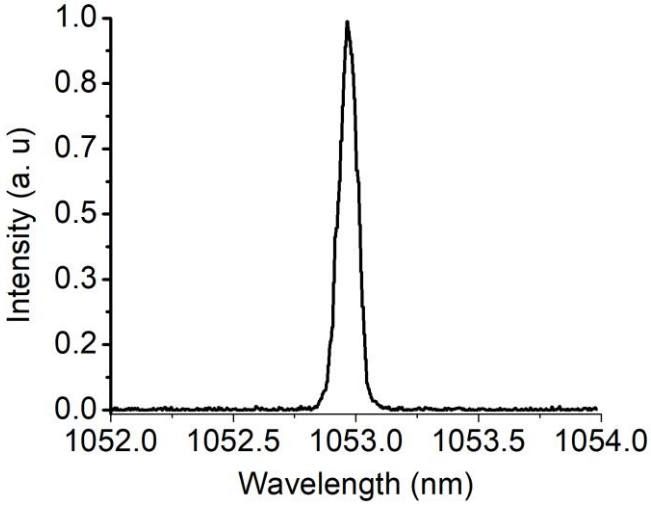

Figure 3.15- CW laser spectrum.

The thermal lensing strength of the 1053 nm Nd:YLF laser was also investigated using the approach and setup discussed in section 3.5 Thermal focal length in the *y*-direction was measured to be ~-3300 mm. However, the thermal lensing focal length in the *x* direction was too weak to be precisely measured. Indeed, it made sense to have a lower thermal lensing strength compared to 1047 nm laser as the *dn/dT* was lower at 1053 nm as was shown in table 2.1.

3.6 Summary

In summary, we demonstrated the first continuous-wave Nd:YLF lasers operating at 1047 nm and 1053 nm which were pumped at 908 nm. As a proof-of-principle experiment the laser generated 850 mW and 625 nmW of average output powers, respectively. The slope efficiencies were ~73.9 % and 46 %, respectively. The results showed that in-band diode pumping at 908 nm is a promising approach to reduce thermal lensing effects and therefore, scale-up the output power.

Chapter 4: Conclusion and future work

In conclusion, we demonstrated the first continuous-wave Nd:YLF laser pumped at 908 nm. As a proof-of-principle experiment the laser generated 850 mW of average output power at 1047 nm with good beam quality and maximum slope efficiency of ~73.9%. The thermal focal length of the thin lens in the middle of the laser crystal were -7290 mm and -2200 mm in horizontal and vertical direction, respectively. Considering the high slope efficiency and approximately twice lower thermal lensing effect we believe that the maximum output power of the developed laser was limited only by the amount of the absorbed pump power. Pump absorption, on the other hand, can be enhanced by using a longer crystal with higher doping concentration.

The results of this work can open a new promising path for power scaling of Nd:YLF lasers in the continuous-wave, mode-locked, and multi-wavelength regimes [45-47,30]. High power Nd:YLF lasers can be also frequency doubled to pump broadly tunable Alexandrite lasers [48-51] for use in nonlinear microscopy [52,53].

Appendix A

ABCD matrix

ABCD matrix analysis is a well-known technique to trace the light path as it travels through the optical system. In this technique, each optical component is described by a 2-by-2 matrix as $\begin{bmatrix} A & B \\ C & D \end{bmatrix}$. The effect of optical elements on the parameters of a Gaussian beam along the *z* direction can be calculated using a complex quantity (q). The q parameter includes the Gaussian beam radius $w(z)$, the wavefront radius of curvature $r(z)$, and the wavelength λ as below:

$$\frac{1}{q(z)} = -i\frac{\lambda}{\pi w(z)^2} + \frac{1}{r(z)} \tag{A.1}$$

The beam characterizes changes as it passes through an optical element. The modified Gaussian beam can be expressed as

$$q' = \frac{Aq+B}{Cq+D} \tag{A.2}$$

where A, B, C, and D are the elements of the optical component. The ABCD matrices related to some of the optical elements are listed below:

Free space	Flat Mirror	Curved Mirror	Crystal	Thin lens
$\begin{bmatrix} 1 & L \\ 0 & 1 \end{bmatrix}$	$\begin{bmatrix} 1 & 0 \\ 0 & 1 \end{bmatrix}$	$\begin{bmatrix} 1 & 0 \\ -2/R & 1 \end{bmatrix}$	$\begin{bmatrix} 1 & d/n \\ 0 & 1 \end{bmatrix}$	$\begin{bmatrix} 1 & 0 \\ -1/2f & 1 \end{bmatrix}$

where L is the distance in the propagation matrix, R is the radius of curvature, d is the crystal length, n is the refractive index and f is the focal length.

The multiplication of the constituent matrices of the cavity can describe the entire optical system. In the resonator design, one should make sure that it is stable. A stable resonator should satisfy equation (A.3),

$$-1 < \frac{A+D}{2} < +1 \tag{A.3}$$

in which *A* and *D* are the elements of the ABCD matrix that describes the entire cavity. The detailed discussion can be found elsewhere [54].

References

[1] K. Sugioka and Y.Cheng, “Ultrafast lasers—reliable tools for advanced materials processing,” Light: Sci Appl. 3, e149 (2014).

[2] T. H. Maiman, “Optical and Microwave-Optical Experiments in Ruby,” Phys. Rev. Lett. 4, 564–566 (1960).

[3] W. Koechner, Solid-State Laser Engineering, (Springer, 2006).

[4] F. D. Zhang, X. H. Zhang, W. Liang, and C. L. Li, “Thermally-boosted pumping of Nd:$LiYF_4$ using Ti:Sapphire laser,” Laser Phys. 21(4), 639–642 (2011).

[5] Y. F. Lü, X. H. Zhang, A. F. Zhang, X. D. Yin, and J. Xia, “Efficient 1047 nm CW laser emission of Nd:YLF under direct pumping into the emitting level,” Opt. Commun. 283(9), 1877–1879 (2010).

[6] J. Jakutis-Neto, J. Lin, N. U. Wetter, and H. Pask, “Continuous-wave Watt-level Nd:YLF/KGW Raman laser operating at near-IR, yellow and lime-green wavelengths,” Opt. Express. 20(9), 9841–9850 (2012).

[7] N. U. Wetter, E. C. Sousa, F. A. Camargo, I. M. Ranieri and S. L. Baldochi, "Efficient and compact diode-side-pumped Nd: YLF laser operating at 1053 nm with high beam quality." J. Opt. A: Pure Appl. Opt. 10(10), 104013 (2008).

[8] C. L. Li, X. H. Zhang, W. Liang, and Z. M. Zhao, “Diode-pumped continuous-wave Nd:YLF laser at 1313 nm,” Laser Phys. 21(2), 340–342 (2011).

[9] D. Geskus, J. Jakutis-Neto, H. M. Pask, and N. U. Wetter, “Intracavity frequency converted Raman laser producing 10 deep blue to cyan emission lines with up to 0.94 W output power,” Opt. Lett. 39(24), 6799–6802 (2014).

[10] N. U. Wetter and A. M. Deana, "Diode-side-pumped Nd:$YLiF_4$ laser emitting at 1053 nm with 53.6% optical efficiency and diffraction-limited beam quality," Laser Phys. Lett. 10(3), 035807 (2013).

[11] D. Sangla, M. Castaing, F. Balembois, and P. Georges, "Highly efficient Nd:YVO_4 laser by direct in-band diode pumping at 914 nm," Opt. Lett. 34(14), 2159–2161 (2009).

[12] J. L. Ma, B. Xiong, L. Guo, P. F. Zhao, L. Zhang, X. C. Lin, J. M. Li, and Q. D. Duanmu, "Low heat and high efficiency Nd:$GdVO_4$ laser pumped by 913 nm," Laser Phys. Lett. 7(8), 579–582 (2010).

[13] M. Nadimi, T. Waritanant, and A. Major, "High power and beam quality continuous-wave Nd:$GdVO_4$ laser in-band diode-pumped at 912 nm," Photon. Res. 5(4), 346–349 (2017).

[14] R. C. Talukder, Md. Z. E. Halim, T. Waritanant, and A. Major, "Multiwatt continuous wave Nd:KGW laser with hot-band diode pumping," Opt. Lett. 41(16), 3810–3812 (2016).

[15] T. Waritanant and A. Major, "Thermal lensing in Nd:YVO_4 laser with in-band pumping at 914 nm," Appl. Phys. B 122(5), 135 (2016).

[16] M. Nadimi, T. Waritanant, and A. Major, "Thermal lensing in Nd:$GdVO_4$ laser with direct in-band pumping at 912 nm," Appl. Phys. B, 124(8), 170 (2018).

[17] T. Waritanant and A. Major, "High efficiency passively mode-locked Nd:YVO_4 laser with direct in-band pumping at 914 nm," Opt. Express 24(12), 12851–12855 (2016).

[18] M. Nadimi, T. Waritanant, and A. Major, "Passively mode-locked high power Nd:$GdVO_4$ laser with direct in-band pumping at 912 nm," Laser Phys. Lett. 15(1), 015001 (2018).

[19] T. Waritanant and A. Major, "Discretely selectable multiwavelength operation of a semiconductor saturable absorber mirror mode-locked Nd:YVO_4 laser," Opt. Lett. 42(17), 3331–3334 (2017).

[20] T. Waritanant and A. Major, "Diode-pumped Nd:YVO_4 laser with discrete multi-wavelength tunability and high efficiency," Opt. Lett. 42(6), 1149–1152 (2017).

[21] Z. Sedaghati, M. Nadimi, A. Major, "An in-band diode-pumped Nd:YLF laser," Photonics North 2018.

[22] Z. Sedaghati, M. Nadimi, A. Major, "Continuous-wave Nd:YLF laser diode-pumped at 908 nm," Photonics West 2019.

[23] Z. Sedaghati, M. Nadimi, A. Major, "Efficient Continuous-Wave Nd:YLF Laser In-Band Diode-Pumped at 908 nm and its thermal lensing," Laser Phys. Lett. (submitted).

[24] Nikon instrument website: URL http://www.microscopyu.com/

[25] Z. Ma, D. Li, J. Gao, N. Wu, K. Du, "Thermal effects of the diode end-pumped Nd:YVO_4 slab," Opt. Commun. 275(1), 179–185 (2007).

[26] P. Markus, "Upconversion-induced heat generation and thermal lensing in Nd:YLF and Nd:YAG," PhD. Thesis, Univerrsity of Southampson, United Kindom (1998).

[27] Castech Crystal Catalog: URL http://www.castech.com/

[28] W. Liang, X. H. Zhang, Z. L. Liang, Y. Q. Liu, and Z. Liang, "Efficient continuous-wave 908 nm Nd:YLF laser emission under direct 880 nm pumping," Laser Phys. 21(2), 320–322 (2011).

[29] Z. Zhang, Q. Liu, M. Nie, E. Ji, and M. Gong, "Experimental and theoretical study of the weak and asymmetrical thermal lens effect of Nd:YLF crystal for σ and π polarizations," Appl. Phys. 120(4), 689–696 (2015).

[30] M.Z.E. Halim, R.C. Talukder, T. Waritanant, A. Major, "Passive mode-locking of a Nd:KGW laser with hot band diode pumping," Laser Phys. 13(10), 105003 (2016).

[31] J. J. Neto, “Low gain Nd:YLF lasers operating in the quasi-three level transition and in Raman lasers”, PhD thesis, Universidade de São Paulo, Brazil (2012).

[32] Z. Lin, Y. Wang, B. Xu, Y. Cheng, H. Xu, and Z. Cai, “Simultaneous dual-wavelength lasing at 1047 and 1053 nm and wavelength tuning to 1072 nm in a diode-pumped a-cut Nd : $LiYF_4$ laser,” Opt. Eng. 54(12), 126114 (2015).

[33] M. Ross, “YAG laser operation by semiconductor laser pumping,“ Proceedings of the IEEE 56(2), 196-197 (1968).

[34] W. P. Risk, “Modeling of longitudinally pumped solid-state lasers exhibiting reabsorption losses,” JOSA B, 5(7), 1412 (1988).

[35] E. Alimohammadian and A. Major, “Modeling of a CW Nd:YVO_4 laser longitudinally pumped by high power VCSEL modules at 808 nm,” Proc. SPIE 8959, 89591 (2014).

[36] P. J. Hardman, W. A. Clarkson, G. J. Friel, M. Pollnau, and D. C. Hanna, “Energy-transfer upconversion and thermal lensing in high-power end-pumped Nd:YLF laser crystals,” IEEE J. Quantum Electron. 35(4), 647–655 (1999).

[37] R. M. El-Agmy and N. Al-Hosiny, “Power scaling of end-pumped Nd:YLF lasers, modeling and experiments,” Optik 140, 584–591 (2017).

[38] Q. Ma, H. Mo, and J. Zhao, “High-energy high-efficiency Nd:YLF laser end-pumped by 808 nm diode,” Opt. Commun. 413, 220–223 (2018).

[39] Rezonator software: URL http://www.rezonator.orion-project.org/

[40] LAS-CAD Software: URL: http://www.las-cad.com/

[41] H. Mirzaeian, S. Manjooran, and A. Major, “A simple technique for accurate characterization of thermal lens in solid state lasers,” Proc. SPIE 9288, 928802 (2014).

[42] B. Pati and G. A. Rines, “Direct-Pumped Nd:YLF Laser,” Proc. Advanced Solid-State Photonics, WB10 (2009).

[42] Y. F. Chen, M. L. Ku, and K. W. Su, “High-power efficient tunable Nd:$GdVO_4$ laser at 1083 nm,” Opt. Lett. 30(16), 2107 (2005).

[44] R. Akbari, H. Zhao, and A. Major, “High-power continuous-wave dual-wavelength operation of a diode-pumped Yb:KGW laser,” Opt. Lett. 41(7), 1601 (2016).

[45] M. Nadimi, T. Waritanant, and A. Major, “Discrete multi-wavelength tuning of a continuous wave diode-pumped Nd:$GdVO_4$ laser,” Laser Phys. Lett. 15(5), 055002 (2018).

[46] T. Waritanant and A. Major, “Dual-wavelength operation of a diode-pumped Nd:YVO_4 laser at the 1064.1 & 1073.1 nm and 1064.1 & 1085.3 nm wavelength pairs,” Appl. Phys. B 124(5), 87 (2018).

[47] A. Major, N. Langford, T. Graf and A. I. Ferguson, “Additive-pulse mode locking of a diode-pumped Nd:KGd(WO4)2 laser,” Appl. Phys. B 75(4-5), 467–469 (2002).

[48] S. Ghanbari and A. Major, “High power continuous-wave Alexandrite laser with green pump,” Laser Phys. 26(7), 075001 (2016).

[49] S. Ghanbari and A. Major, “High power continuous-wave dual-wavelength Alexandrite laser,” Laser Phys. Lett. 14(10), 105001 (2017).

[50] S. Ghanbari, R. Akbari and A. Major, “Femtosecond Kerr-lens mode-locked Alexandrite laser,” Opt. Express 24(13), 14836-14840 (2016).

[51] S. Ghanbari, K.A. Fedorova, A.B. Krysa, E.U. Rafailov, and A. Major, "Femtosecond Alexandrite laser passively mode-locked by an InP/InGaP quantum-dot saturable absorber," Opt. Lett. 43(2), 232-234 (2018).

[52] L. B. Mostaço-Guidolin, A. C-T. Ko, D. P. Popescu, M. S. D. Smith, E. K. Kohlenberg, M. Shiomi, A. Major, M. G. Sowa, “Evaluation of texture parameters for the quantitative description of multimodal nonlinear optical images from atherosclerotic rabbit arteries,” Physics in Medicine and Biology 56(16), 5319–5334 (2011).

[53] A. Major, R. Cisek and V. Barzda, “Development of diode-pumped high average power continuous-wave and ultrashort pulse Yb:KGW lasers for nonlinear microscopy,” Proc. SPIE 6108, 61080Y (2006).

[54] B. E. A. Saleh and M. C. Teich, Fundamentals of Photonics, 2nd Edition, (John Wiley & Sons, 2007).